The Journal of Clinical Pharmacology
2020, 60(12) 1629–1641

DOI: 10.1002/jcph.1680

Population Pharmacokinetic Analysis of Quizartinib in Healthy Volunteers and Patients With Relapsed/Refractory Acute Myeloid Leukemia

Dongwoo Kang, PhD[1], Elizabeth Ludwig, PharmD[2], David Jaworowicz, PhD[2], Hannah Huang, PhD[2], Jill Fiedler-Kelly, MS, FISoP[2], Jorge Cortes, MD[3], Siddhartha Ganguly, MD[4], Samer Khaled, MD[5], Alwin Krämer, MD[6], Mark Levis, MD, PhD[7], Giovanni Martinelli, MD[8], Alexander Perl, MD[9], Nigel Russell, MD[10], Malaz Abutarif, MD, PhD[1], Youngsook Choi, MD[1], Jeanne Mendell, PhD, MPH[1], and Ophelia Yin, PhD[1]

Abstract

Quizartinib is an FMS-like tyrosine kinase 3 (FLT3) inhibitor that has shown robust clinical activity in patients with *FLT3*-internal tandem duplication–mutated relapsed/refractory acute myeloid leukemia (AML). This analysis evaluated the population pharmacokinetics (PK) of quizartinib and its active metabolite, AC886, in a pooled analysis of data from 649 healthy volunteers or patients with AML from 8 clinical trials including the phase 3 QuANTUM-R study. Quizartinib was given as a single dose or multiple once-daily doses of 20, 30, 60, or 90 mg. Nonlinear mixed-effects modeling was performed using observed concentrations of quizartinib and AC886. Strong CYP3A inhibitor use resulted in an 82% increase in the area under the curve (AUC) and a 72% increase in the maximum concentration (C_{max}) of quizartinib. Albumin level, age, and body surface area were statistically significant covariates on quizartinib PK. However, their individual effects on quizartinib AUC and C_{max} were <20%. For AC886, strong CYP3A inhibitor use, body surface area and black/African American race were significant covariates. Except for strong CYP3A inhibitor use, the effects on the overall exposure (AUC of quizartinib + AC886) were <20%. The population PK model provided an adequate description of the observed concentrations of quizartinib and AC886 in both healthy volunteers and patients with AML. Only concomitant use of strong CYP3A inhibitors had a clinically meaningful effect on quizartinib PK exposure.

Keywords

AC886, acute myeloid leukemia, population pharmacokinetics, quizartinib, relapsed/refractory

FMS-like tyrosine kinase 3 (FLT3) is expressed in hematopoietic progenitor cells and is mutated in approximately 30% of patients with acute myeloid leukemia (AML).[1,2] The *FLT3*-internal tandem duplication (ITD) mutation represents the most common type of *FLT3* mutation and is associated with high relapse rates, decreased response to salvage therapy, and shorter overall survival.[1-4]

Quizartinib is an oral, once-daily, highly potent, and selective type II FLT3 inhibitor that has shown high levels of clinical activity in patients with *FLT3*-ITD-positive relapsed/refractory AML.[5,6] Single-agent quizartinib treatment demonstrated clinically meaningful overall survival benefit in patients with relapsed/refractory *FLT3*-ITD AML compared with salvage chemotherapy, with a 24% reduction in the risk of death in the phase 3 QuANTUM-R (AC220-007) trial.[7]

[1]Daiichi Sankyo, Inc., Basking Ridge, New Jersey, USA
[2]Cognigen Corporation, a Simulations Plus company, Buffalo, New York, USA
[3]The University of Texas MD Anderson Cancer Center, Houston, Texas, USA
[4]The University of Kansas Cancer Center, Fairway, Kansas, USA
[5]City of Hope, Arcadia, California, USA
[6]Clinical Cooperation Unit Molecular Hematology/Oncology, Department of Internal Medicine V, University of Heidelberg, Heidelberg, Germany
[7]Sidney Kimmel Comprehensive Cancer Center at Johns Hopkins University, Baltimore, Maryland, USA
[8]Istituto Scientifico Romagnolo per lo Studio e la Cura dei Tumori (IRST) IRCCS, Meldola, Italy
[9]Division of Hematology and Oncology, Abramson Cancer Center of the University of Pennsylvania, Philadelphia, Pennsylvania, USA
[10]Centre for Clinical Haematology, Nottingham University Hospitals NHS Trust, Nottingham, UK

Submitted for publication 31 March 2020; accepted 1 June 2020.

Corresponding Author:
Dongwoo Kang, PhD, Daiichi Sankyo, Inc., 211 Mt. Airy Road, Basking Ridge, NJ 07920
Email: dkang@dsi.com

[Correction added on 14 September 2020, after first online publication: in the abstract, "patient status" is deleted from "For AC886, strong CYP3A … were significant covariates." and "and AC886" is deleted from "Only concomitant use of strong … exposure".]

[The copyright line for this article was changed on 28 September, 2020 after original online publication.]

Following oral administration, quizartinib is rapidly absorbed and is primarily metabolized by cytochrome P450 (CYP) 3A to form the metabolite AC886, which is further metabolized by CYP3A.[8,9] Quizartinib and AC886 have similar pharmacokinetics (PK) and have demonstrated potent and selective inhibition of FLT3 kinase in the context of other FLT3 inhibitors, with dissociation constant (Kd) values of 3.3 and 1.1 nM for quizartinib and AC886, respectively.[10,11] A drug-drug interaction study of quizartinib with ketoconazole or fluconazole showed that strong CYP3A inhibitors increase quizartinib exposure by approximately 2-fold.[8] Because quizartinib concentration is highly correlated with QTc prolongation,[12] a reduction in the quizartinib dose is warranted when concomitantly administered with a strong CYP3A inhibitor. A phase 2 study evaluating quizartinib 30 and 60 mg/day showed high levels of clinical activity at both doses, with a numerically higher overall response rate, duration of composite complete remission, and median overall survival observed with the higher dose.[6,13] On the basis of these results, the dosing set for the phase 3 QuANTUM-R study started at 30 mg/day and increased to 60 mg/day after 2 weeks if the QT interval corrected using Fridericia's formula (QTcF) was ≤ 450 milliseconds; however, patients receiving a concurrent strong CYP3A inhibitor initiated quizartinib at 20 mg/day, with an increase to 30 mg/day.[7]

This report describes a population PK analysis of quizartinib and AC886 using pooled data from 8 phase 1, 2, or 3 clinical trials in which quizartinib was administered as single or multiple daily doses of 20, 30, 60, or 90 mg dihydrochloride salt (equivalent to 17.7, 26.5, 53.0, and 79.5 mg free base, respectively). The analysis included an exploratory data analysis, base structural model development, evaluation of covariate effects, and final model evaluation, with the objectives of characterizing the population PK characteristics of both quizartinib and AC886, including identification of key covariates affecting the variability of quizartinib or AC886 PK.

Methods

All study protocols were reviewed and approved by the respective institutional review board or ethics committee at each site. All patients provided written informed consent according to the Declaration of Helsinki and Good Clinical Practice.

Data

Data for the population PK analysis were from 6 phase 1, 1 phase 2, and 1 phase 3 study (QuANTUM-R). A brief description of each study, along with sample size and detailed PK sampling time points, is presented in Table 1. Quizartinib was given as a single dose or multiple doses of 20, 30, 60, and 90 mg in salt form (equivalent to 17.7, 26.5, 53.0, and 79.5 mg free base, respectively). The phase 1 studies of healthy volunteers included administration of only single doses of quizartinib, whereas in studies of patients with AML, quizartinib was administered as multiple daily doses (Table 1). In QuANTUM-R, the starting dose was 30 mg/day, followed by an increase to 60 mg/day after 2 weeks if QTcF was ≤450 milliseconds to reduce the risk of QT prolongation events. Patients concurrently receiving a strong CYP3A inhibitor initiated quizartinib at 20 mg/day, with an increase to 30 mg/day after 2 weeks if QTcF was ≤450 milliseconds. Quizartinib was administered as 20- or 30-mg tablets except in studies AC220-014 and 2689-CL-0011, in which an oral solution was also administered. Patients in study 2689-CL-2004 received oral solution only.

Demographic and clinical characteristics used as covariates in the model or as participant descriptors included sex, race, baseline age (years), baseline weight (kg), baseline body surface area (m^2), baseline creatinine clearance, baseline liver function tests (aspartate aminotransferase [AST], alanine aminotransferase [ALT], alkaline phosphatase [ALP], and total bilirubin [TBIL]), baseline serum albumin (ALB), FLT3-ITD status (positive or negative), concomitant medications (CYP3A inhibitors, CYP3A inducers, and gastric acid-reducing agents [proton pump inhibitors, H_2 antagonists, and antacids]), and patient status (ie, patients with AML or healthy volunteers). All covariates were baseline values except for concomitant medications, which were evaluated as time-varying covariates.

For the population pk modeling, the actual dates and times of dosing and pk samples were used to create the NONMEM analysis data set. The analysis data set was prepared using clinical study data tabulation model data.

Bioanalytical Methods

Plasma concentrations of quizartinib and AC886 were determined using 2 liquid chromatography-tandem mass spectrometry 2-analyte assay methods, developed and validated at BASi (West Lafayette, Indiana). The first assay was used for studies 2689-CL-0011, AC220-014, AC220-015, 2689-CL-2004, and QuANTUM-R and had a calibration curve ranging from 2 to 2000 ng/mL and lower limits of quantitation of 2 ng/mL for both quizartinib and AC886. The second assay was used for studies AC220-016, AC220-018, and AC220-019. This assay was the same as the first, except that it had a lower calibration range of 0.5 to 500 ng/mL and lower limits of quantification of 0.5 ng/mL for both quizartinib and AC886. Cross-validation was conducted between the 2 assays using

Table 1. Summary of the Study Design of the 8 Studies Included in the Population PK Analysis

Study	Phase	n	Number of PK Samples		Dose Regimen	Study Population	Description	PK Sampling Times
			Quizartinib	AC886				
AC220-014	1	80	1528	1439	Single dose of 60-mg solution or 30-, 60-, or 90-mg tablets	Healthy volunteers	Relative bioavailability and dose proportionality	0, 0.25, 0.5, 1, 2, 3, 4, 5, 6, 8, 12, 24, 36, 48, 72, 96, 120, 144, 168, 240, 312, 384, and 480 hours postdose
AC220-015[8]	1	89	1970	1543	Single dose of 30 mg	Healthy volunteers	Drug-drug interaction with ketoconazole, fluconazole	0, 0.25, 0.5, 1, 2, 3, 4, 5, 6, 8, 12, 24, 36, 48, 72, 96, 120, 144, 168, 192, 216, 288, 360, 432, and 504 hours postdose
AC220-016	1	30	686	654	Single dose of 30 mg	Healthy volunteers	Hepatic impairment study	0, 0.25, 0.5, 1, 2, 3, 4, 5, 6, 8, 12, 24, 36, 48, 72, 96, 120, 144, 168, 192, 216, 288, 360, 432, and 504 hours postdose
AC220-018[19]	1	62	1422	1338	Single dose of 30 mg	Healthy volunteers	Drug-drug interaction with lansoprazole	0, 0.25, 0.5, 1, 2, 3, 4, 5, 6, 8, 12, 24, 36, 48, 72, 96, 120, 144, 168, 192, 216, 288, 360, 432, and 504 hours postdose
AC220-019[27]	1	64	1374	1259	Single dose of 30 mg	Healthy volunteers	Food effect study	0, 0.25, 0.5, 1, 2, 3, 4, 5, 6, 8, 12, 24, 36, 48, 72, 96, 120, 144, 168, 192, 216, 288, 360, 432, and 504 hours postdose
2689-CL-0011[28]	1	13	243	239	Multiple daily doses of 30, 40, 60, or 90 mg	Patients with AML	Maintenance dosing following transplantation for relapsed/refractory AML	0, 1, 2, 4, 6, and 24 hours postdose on PK sampling days (cycle 1 days 1 and 15). Less frequently, 1 or 2 samples on other days.
2689-CL-2004[6]	2b	72	1090	1070	Multiple daily doses of 30 or 60 mg	Patients with AML	Dose-ranging study in AML	0, 1, 2, 4, 6, and 24 hours postdose on PK sampling days (cycle 1 days 1 and 15). Less frequently, 1 or 2 samples on other days.
QuANTUM-R (AC220-007)[7]	3	239	3457	3346	Multiple daily doses of 20, 30, or 60 mg	Patients with AML	Phase 3 study in relapsed/refractory AML	0, 1, 2, 4, 6, and 24 hours postdose on PK sampling days (cycle 1 days 1 and 15). Less frequently, 1 or 2 samples, on other days.
Total		649	11 770	10888				

AML, acute myeloid leukemia; PK, pharmacokinetic.

the quality control samples at concentrations of 6 and 1500 ng/mL. Precision was similar for both quizartinib (first assay, <5.0%; second assay, <3.2%) and AC886 (first assay, <5.3%; second assay, <2.1%). Accuracy was also comparable between the 2 assays (quizartinib, <2.5% versus <3.3%; AC886, <1.7% versus <6.0%).

Population Pharmacokinetic Modeling Analysis

The first-order conditional estimation method as implemented in NONMEM V.7.3.0 (ICON Development Solutions, Elliott City, Maryland) was used for model estimation. All data preparation, statistical analyses, and data presentation were performed using SAS version 9.4 (SAS Institute, Cary, North Carolina) or KIWI version 2 software (Cognigen Corporation, Buffalo, New York).

For the base model determination, several multicompartment structural models were explored. A first- and/or zero-order absorption process with or without an absorption lag time was tested for appropriate description of quizartinib absorption.

For model fitting of both quizartinib and AC886 concentrations, simultaneous and 2-step sequential analyses were explored. For the latter, AC886 concentrations were modeled conditioned on the quizartinib PK model, in which all quizartinib model parameters were fixed to the empirical Bayesian PK parameter estimates for individual participants.

Covariates were initially selected based on univariate analysis and clinical relevance. The selected covariates were then tested one at a time using stepwise addition at a significance level of $P < .01$. After the full model was constructed, a backward elimination process was applied ($P < .001$) to ensure the significance of selected covariates in the final model.

The effect of continuous covariates was described using a power model as $\text{TVP} = \theta_1 \cdot (X_i/X_{ref})^{\theta 2}$, where X_i is the value of the covariate of interest, X_{ref} is the centering value (eg, median) of that covariate, TVP is the typical value of a PK parameter, θ_1 is the typical parameter value for an individual with the median value of the covariate, and θ_2 is the typical value estimate describing the change in the log parameter value per unit change in the log of a particular covariate.

For dichotomous covariates such as sex, the fractional change in the typical parameter value was modeled as an incremental change in the typical parameter value as $\text{TVP} = \theta_1 \cdot (1 + \text{IND} \cdot \theta_2)$, where θ_1 is the typical parameter value for a reference individual, θ_2 is the fractional change in the typical value for a covariate category, and IND is the indicator function (IND = 1 if the covariate is present and IND = 0 if the covariate is absent). For categorical variables with >2 groups, indicator variables were created to evaluate the effect of each group compared with that of the group defined as the reference population. Additional fractional terms were used for each separate indicator variable.

Model selection was based on the value of the objective function, goodness-of-fit plots, precision in parameter estimates, and scientific plausibility. Goodness-of-fit diagnostic plots and prediction-corrected visual predictive checks (pcVPCs) were inspected for major steps of model building.

Simulation for Covariate Effects

To illustrate the effect of each individual covariate on quizartinib and AC886 steady-state PK profiles in patients with AML, simulations were performed by varying each covariate value one at a time while keeping other covariates constant (ie, categorical covariates were set at the reference categories, and continuous covariate values were set to the median values in the AML patient population). Quizartinib and AC886 steady-state exposures ($AUC_{0\text{-}24,ss}$ and $C_{max,ss}$) at the 5th, 25th, 75th, and 95th percentiles of the continuous covariates or at each level of the categorical covariates were simulated and then compared with the exposure estimates for the reference patient with AML.

Results

Data

The population PK analysis data set consisted of 11 770 quizartinib and 10 888 AC886 plasma samples from 649 participants, of whom 325 were healthy volunteers and 324 were patients with AML (Table 1). Healthy volunteers, with a median age of 33 years, were younger than patients with AML, who had a median age of 55 years (Table 2). Just more than half the study population was male (57.9%), and 68.7% were white (Table 2). Patients with AML had lower median baseline ALB level (3.7 versus 4.4 g/dL) and lower baseline red blood cell count (3.0×10^{12}/L versus 4.8×10^{12}/L) than healthy volunteers. The dose-normalized concentration profiles of quizartinib (Figure 1A) and AC886 (Figure 1B) in patients with AML suggested some extent of accumulation on multiple administrations of quizartinib. Steady state was achieved by approximately cycle 1 day 15, as seen from the profiles of trough concentrations over time (Figure 1C). The median accumulation ratio was 4.8 for quizartinib and 8.4 for AC886, estimated from patients from the QuANTUM-R study.

Model Building

Simultaneous and sequential modeling approaches were considered in building the population PK models for quizartinib and AC886. After thorough exploration, a 2-step sequential analysis was selected as the preferred method because long computational times and persistent numerical problems encountered with the simultaneous model were prohibitive during early model development. In the sequential analysis used to model AC886 concentrations, individual quizartinib parameters were fixed to post hoc values obtained from the final quizartinib population PK model. Because only PK data from oral administration of quizartinib were available for this analysis, the fraction of formation from quizartinib to AC886 was fixed to avoid the commonly known unidentifiability issue.[14] A fixed value of 0.5 was used because the geometric mean AUC ratio of quizartinib to AC886 in the phase 2 study was 0.5.

Quizartinib Population PK Model

A 3-compartment PK model with zero-order and first-order absorption and a lag time represented the best fit for the quizartinib concentration data (Figure 2). A log-normal distribution model was used for interindividual variability (IIV), and a combined proportional and additive error model was applied to the untransformed concentrations of quizartinib, with patient-specific and

Table 2. Baseline Demographic and Clinical Characteristics of Healthy Volunteers and Patients With AML Included in the Study Analysis

Characteristics	Healthy Volunteers (n = 325)	Patients With AML (n = 324)	Total (N = 649)
Age (years), median (range)	33 (18-66)	55 (19-81)	44 (18-81)
Sex, n (%)			
Male	216 (66.5)	160 (49.4)	376 (57.9)
Female	109 (33.5)	164 (50.6)	273 (42.1)
Race, n (%)			
White	199 (61.2)	247 (76.2)	446 (68.7)
Black or African American	105 (32.3)	12 (3.7)	117 (18.0)
Asian	4 (1.2)	27 (8.3)	31 (4.8)
American Indian or Alaska Native	6 (1.9)	1 (0.3)	7 (1.1)
Native Hawaiian or other Pacific Islander	1 (0.3)	0 (0)	1 (0.2)
Other	10 (3.1)	8 (2.5)	18 (2.8)
Unknown	0 (0)	29 (9.0)	29 (4.5)
BSA (m^2), median (range)	1.9 (1.4-2.5)	1.9 (1.3-2.8)	1.9 (1.3-2.8)
Weight (kg), median (range)	76.9 (48.1-112)	72.0 (39.5-153)	74.4 (39.5-153)
Red blood cell count (10^{12}/L), median (range)	4.8 (3.5-6.1)	3.0 (0.4-5.1)	3.7 (0.4-6.1)
Liver function tests, median (range)			
ALB (g/dL)	4.4 (3.3-5.2)	3.7 (2.1-4.8)	4.1 (2.1-5.2)
ALP (U/L)	65 (31-221)	86 (28-507)	73 (28-507)
ALT (U/L)	17 (6-201)	24 (2-224)	19 (2-224)
AST (U/L)	20 (10-261)	24 (3-688)	21 (3-688)
TBIL (mg/dL)	0.5 (0.1-3.4)	0.5 (0.1-1.6)	0.5 (0.1-3.4)
eGFR (mL/min/1.73 m^2), median (range)	91.7 (49.1-379)	94.3 (21.2-256)	92.8 (21.2-379)
Concomitant CYP3A inhibitor, n (%)			
Strong CYP3A inhibitors	29 (8.9)	93 (28.7)	122 (18.8)
Moderate CYP3A inhibitors	30 (9.2)	106 (32.7)	136 (21.0)
Weak or no CYP3A inhibitors	266 (81.8)	125 (38.6)	391 (60.2)

ALB, albumin; ALP, alkaline phosphatase; ALT, alanine aminotransferase; AML, acute myeloid leukemia; AST, aspartate aminotransferase; BSA, body surface area; CYP, cytochrome P450; eGFR, estimated glomerular filtration rate; SD, standard deviation; TBIL, total bilirubin.

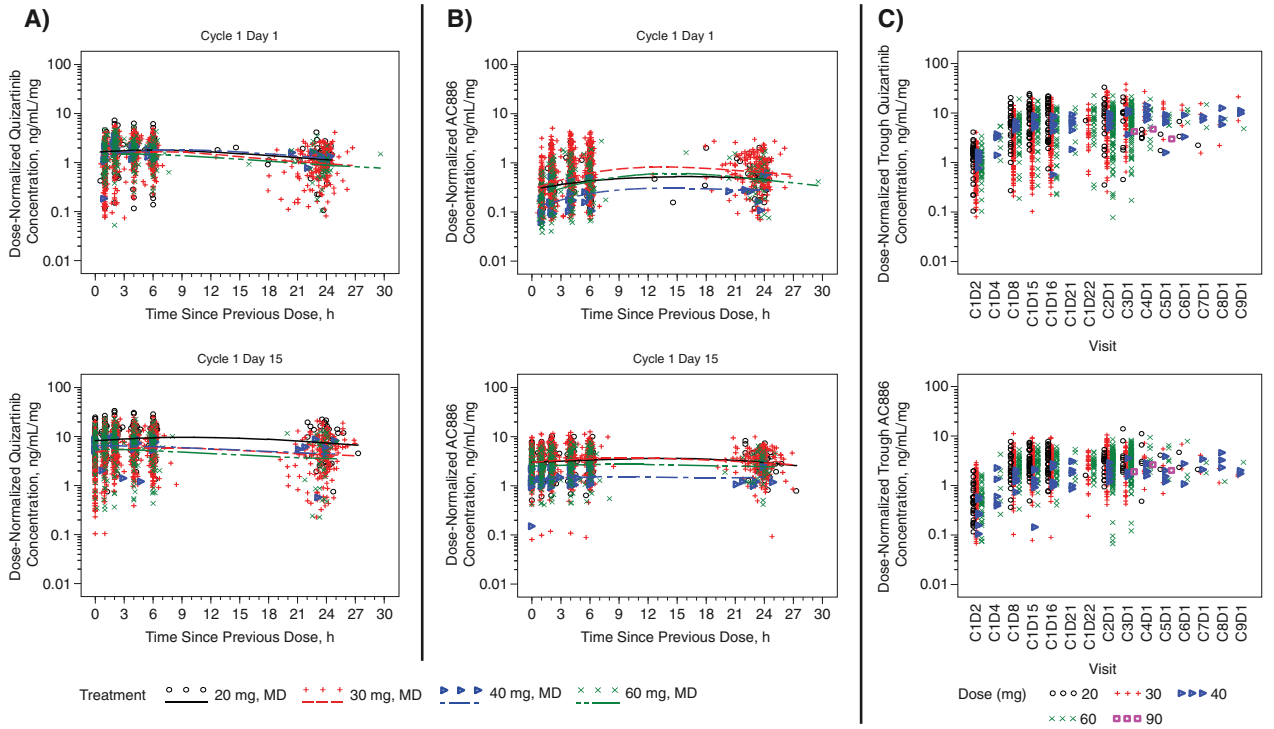

Figure 1. Dose-normalized concentration profile of quizartinib (A) and AC886 (B) by quizartinib dose in patients with AML, shown per time since previous dose. Dose-normalized trough concentrations of quizartinib and AC886 (C), shown per visit days. The lines represent smoothing lines of the data. MD, multiple doses.

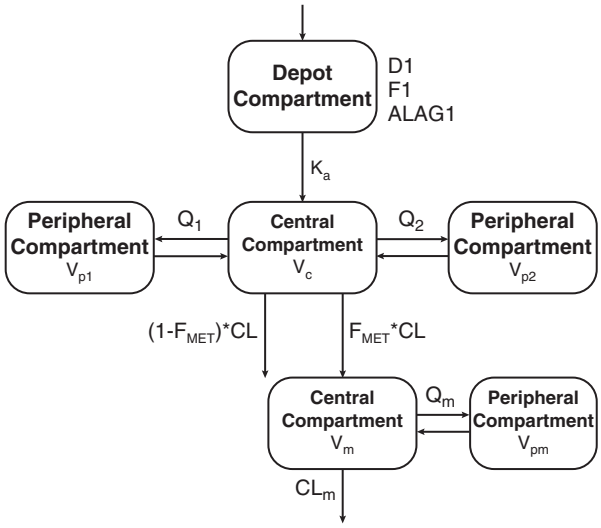

Figure 2. Final PK model diagram. D1, duration of zero-order input; F1, bioavailability; ALAG1, absorption lag time; K_a, first-order absorption rate constant; V_c, central volume of distribution; V_{p1}, peripheral volume of distribution 1; V_{p2}, peripheral volume of distribution 2; Q_1, intercompartmental clearance 1; Q_2, intercompartmental clearance 2; CL, clearance; F_{MET}, parent-to-metabolite conversion fraction; V_m, central volume of distribution for metabolite; V_{pm}, peripheral volume of distribution for metabolite; Q_m, intercompartmental clearance for metabolite; CL_m, metabolite clearance.

healthy volunteer-specific proportional error terms, to describe residual variability (RV).

The covariate models were built using the process of stepwise addition followed by backward elimination. Identified significant covariates were patient status on clearance (CL), V_c, and V_{p1}; strong CYP3A inhibitor on CL and relative F1; and ALB and body surface area (BSA) on V_c. Inclusion of these covariate effects improved the model fit to the observed data.

After the initial model-building phase, a second step was undertaken to assess other considerations to potentially improve the quizartinib PK model and to enhance model fit. Specifically, food effect was evaluated on absorption parameters, relative bioavailability was estimated for relevant groups, and the effects of interoccasion variability (IOV) and patient status (patients with AML versus healthy volunteers) were assessed on various structural parameters.

The IOV was systematically tested on all applicable PK parameters, resulting in the estimation of IOV in F1, CL, and V_c. This characterization of the random variability in PK parameters over time considerably improved the prediction of quizartinib concentrations collected across different occasions in the multiple-dose phase 3 studies and also corroborated the lack of any time-dependent changes in quizartinib PK. The magnitude of IOV was estimated to be 22.6%, 40.9%, and 20.3% for F1, CL, and V_c, respectively. Exposure of quizartinib appeared lower in patients with AML than in healthy volunteers. Lower exposure was initially characterized by higher CL, V_c, and V_{p1} (75%, 36%, and 102% increases, respectively, in patients with AML). Given that the effects were in the same direction, lower quizartinib bioavailability in patients with AML than in healthy volunteers could also account for the lower exposure rather than an inherent difference in the distribution and/or disposition of the drug. Therefore, a relative bioavailability (F1) parameter was incorporated into the model (in lieu of patient differences in CL and volume) to describe the difference in bioavailability between the AML patient population and healthy volunteers. A 40.1% reduction in bioavailability was estimated for patients with AML relative to healthy volunteers. In addition, a fractional change for patient status on CL was estimated and described an 8.2% increase in CL for patients with AML versus healthy volunteers.

To assess the food effect on quizartinib PK, data from a phase 1 food effect study (AC220-019) were included in the population PK analysis data set. However, because of lack of comprehensive food data (eg, food intake, type of meal, and timing) in other studies included in the analysis, food effect was estimated only for individuals from the AC220-019 study. On the basis of these data, a 51.2% decrease in k_a and 5.1% increase in F1 were estimated when quizartinib was administered under fed conditions versus fasted conditions. These model-based estimates were consistent with the observed data from the study.

Because the observed T_{max} occurs sooner (eg, 2 hours) in patients with AML than in healthy volunteers, k_a was estimated separately for healthy volunteers and for patients with AML. The estimates indicated that the absorption rate for quizartinib was generally higher in patients with AML (1.68 1/h) than in healthy volunteers (0.874 1/h).

The significant covariates included in the final quizartinib population PK model were patient status and fed status on k_a; patient status and concomitant strong CYP3A inhibitor use on CL, BSA, and ALB on V_c; BSA and age on V_{p1}; BSA on Q_1; and patient status, fed status (study AC220-019), and concomitant strong CYP3A inhibitor use on F1. Detailed parameter values are presented in the Final Model section and in Table 3.

AC886 Population PK Model

A 2-compartment PK model provided the best fit for the AC886 concentration data (Figure 2). Log-transformed concentrations were modeled with AML patient-specific and healthy volunteer-specific additive RV terms. As with the quizartinib population PK model, a log-normal distribution was used for IIV. Separate IIV terms for healthy volunteers and for patients with AML were included for the apparent clearance of

Table 3. Population PK Parameter Estimates for Quizartinib

	Final Parameter Estimate		Magnitude of Interindividual Variability	
Parameter	Population Mean	% RSE	Final Estimate	% RSE
CL (apparent clearance for parent), L/h	2.77	2.04	55.1% CV	6.65
CL (fractional change[a] in CL for patients)	0.0820	29.1		
CL (fractional change in CL for strong CYP3A inhibitors)	−0.441	3.86		
V_c (apparent volume of distribution for central compartment), L	194	1.89	27.6% CV	8.39
V_c (exponent of [ALB/4.1] for V_c)	−0.725	12.6		
V_c (exponent of [BSA/1.9] for V_c)	1.46	7.16		
Q_1 (intercompartmental clearance 1), L/h	27.9	3.14	24.8% CV	23.3
Q_1 (exponent for BSA on Q_1)	0.970	23.3		
V_{p1} (apparent volume of distribution for peripheral compartment 1), L	170	2.53	39.7% CV	10.6
V_{p1} (exponent for BSA on V_{p1})	1.50	10.9		
V_{p1} (exponent for age on V_{p1})	0.453	10.7		
Q_2 (intercompartmental clearance 2), L/h	0.567	4.87	NE	NA
V_{p2} (apparent volume of distribution for peripheral compartment 2), L	39.3	1.86	NE	NA
K_a (first-order absorption constant for healthy participants), 1/h	0.874	3.00	38.5% CV	9.14
K_a (first-order absorption constant for patients), 1/h	1.68	0.484		
K_a (fractional change in K_a for fed status [019 only])	−0.512	8.75		
D1 (duration of zero-order input to depot compartment), h	0.708	3.86	69.3% CV	8.69
F1 (relative F1 for patients)	0.599	3.26	34.8% CV	13.2
F1 (fractional change in F1 for strong CYP3A inhibitors)	0.136	14.6		
F1 (relative F1 for study 019 [fasted])	0.913	1.86		
F1 (fractional change in study 019 F1 for fed)	0.0509	52.0		
ALAG1 (absorption lag time), h	0.205	4.09	62.0% CV	7.36
IOV in F1 on occasion 1	22.6% CV	20.6	NA	NA
IOV in F1 on occasion 3				
IOV in CL on occasion 1	40.9% CV	7.85	NA	NA
IOV in CL on occasion 2				
IOV in CL on occasion 3				
IOV in CL on occasion 4				
IOV in V_c on occasion 1	20.3% CV	17.0	NA	NA
IOV in V_c on occasion 2				
IOV in V_c on occasion 3				
IOV in V_c on occasion 4				
RV (healthy volunteer CCV component)	0.00563	3.76	49.4-7.50% CV[b] F (2-1000 ng/mL)	NA
RV (patient CCV component)	0.0376	7.10	52.6-19.4% CV[c] F (2-1000 ng/mL}	NA
RV (healthy volunteer additive component)	0.956	4.45		NA
RV (patient additive component)	0.956	SAME		NA
Minimum value of the objective function = 72 031.19				

ALB, albumin; BSA, body surface area; CCV, constant coefficient of variation; % CV, coefficient of variation expressed as a percent; CYP3A, cytochrome P450 3A; F, prediction; IOV, interoccasion variability; NA, not applicable; NE, not estimated; RSE, relative standard error expressed as a percent; RV, residual variability.

[a]The fractional change in the typical parameter value was modeled as an incremental change in the typical parameter value as, for this case: $CL_i = 2.77 \times [1 + (0.0820 \times flag_{PATIENT_i})]$.

[b]The residual variability (% CV) was calculated using the following equation: (SQRT[$F^2 \times 0.00563$+0.956]/F) × 100. Residual variability is 49.4% CV for predicted concentration value of 2 ng/mL and 7.50% CV for predicted concentration value of 1000 ng/mL.

[c]The residual variability (% CV) was calculated using the following equation: (SQRT[$F^2 \times 0.0376$+0.956]/F) × 100. Residual variability is 52.6% CV for predicted concentration value of 2 ng/mL and 19.4% CV for predicted concentration value of 1000 ng/mL.

the metabolite (CL_m) to capture the different magnitudes of variability in the 2 populations.

The AC886 covariate models were built using the same process that was used to develop the quizartinib model. Significant covariate effects on AC886 PK included body surface area, black/African American race, and strong CYP3A inhibitor use on CL_m, and strong CYP3A inhibitor use and patient status on V_m. Detailed parameter values are presented in Table 4.

Final Population PK Models

The final quizartinib population PK model equations to describe parameter-covariate relationships are shown below in equations 1-7.

$$k_{a_i} = 0.874 \times (1 - flag_{PATIENT_i}) \times (1 + flag_{FED_i} \times (-0.512)) + 1.68 \times flag_{PATIENT_i} \quad (1)$$

Table 4. Population PK Parameter Estimates for AC886

Parameter	Final Parameter Estimate		Magnitude of Interindividual Variability	
	Population Mean	% RSE	Final Estimate	% RSE
CL_m (apparent clearance for metabolite), L/h	4.09	3.07	NE	NA
CL_m (power of BSA in CL_m)	1.60	12.5		
CL_m (fractional change in CL_m for race black)	0.586	14.1		
CL_m (fractional change in CL_m for strong CYP3A inhibitors)	0.106	27.7		
FMET (fraction of quizartinib converted to AC886)	0.500	FIXED	NE	NA
V_{cm} (apparent central volume of distribution for metabolite), L	4.95	8.27	117% CV	8.30
V_{cm} (fractional change in V_{cm} for strong CYP3A inhibitors)	1.92	19.3		
V_{pm} (apparent peripheral volume of distribution for metabolite), L	70.6	1.06	NE	NA
Q_m (intercompartmental clearance for metabolite), L/h	3.29	1.28	NE	NA
IIV in CL_m in healthy volunteers	NA	NA	45.9% CV	8.50
IIV in CL_m in patients	NA	NA	64.1% CV	8.62
Residual variability for healthy volunteer studies[a]	0.0690	0.791	0.263 SD	NA
Residual variability for studies of patients with AML[a]	0.169	1.02	0.412 SD	NA
Minimum value of the objective function = −10 302.217				

BSA, body surface area; % CV, coefficient of variation expressed as a percent; CYP, cytochrome P450; IIV, interindividual variability; NA, not applicable; NE, not estimated; % RSE, relative standard error expressed as a percent.

[a]Residual variability is in units of variance: residual variability of 0.0690 for healthy volunteer studies corresponds to 26.3% CV and of 0.169 for studies of patients with AML corresponds to 41.2% CV.

$$F1_i = [1 \times (1 - flag_{PATIENT_i}) + 0.599 \times flag_{PATIENT_i}] \times (1 + flag_{STRCYP_i} \times 0.136) \quad (2)$$

$$F1_{S19_i} = 0.913 \times (1 + flag_{FED_i} \times 0.0509) \quad (3)$$

$$CL_i = 2.77 \times [1 + (0.082 \times flag_{PATIENT_i}) + ((-0.441) \times flag_{STRCYP_i})] \quad (4)$$

$$V_{c_i} = 194 \times \left(\frac{ALB_i}{4.1}\right)^{-0.725} \times \left(\frac{BSA_i}{1.9}\right)^{1.46} \quad (5)$$

$$V_{p1_i} = 170 \times \left(\frac{BSA_i}{1.9}\right)^{1.50} \times \left(\frac{Age_i}{44}\right)^{0.453} \quad (6)$$

$$Q_{1_i} = 27.9 \times \left(\frac{BSA_i}{1.9}\right)^{0.970} \quad (7)$$

where k_{a_i} is the first-order absorption rate constant (1/h) in the *i*th participant; $flag_{PATIENT_i}$ is the indicator variable for patient status (0 for healthy participant, 1 for patient with AML); $flag_{FED_i}$ is the indicator variable for fed/fasted status (0 for fasted, 1 for fed); $F1_i$ is the F1 in the *i*th participant (not including participants in AC220-019); $F1_{S19_i}$ is the F1 in the *i*th participant enrolled in AC220-019; $flag_{STRCYP_i}$ is the indicator variable for strong CYP3A inhibitor use (0 for no strong CYP3A inhibitor use, 1 for strong CYP3A inhibitor use); CL_i is the quizartinib clearance (L/h); V_{c_i} is the quizartinib central volume of distribution (L); ALB_i is the serum albumin (g/dL); BSA_i is the body surface area (m^2); V_{p1_i} is the quizartinib volume of peripheral compartment 1 (L); Age_i is the age (years); and Q_{1_i} is the quizartinib apparent intercompartmental clearance between the central compartment and peripheral compartment 1.

The absorption rate for quizartinib was predicted to be higher in patients with AML (1.68 1/h) than in healthy volunteers (0.874 1/h). A 40.1% reduction in bioavailability and an 8.2% increase in CL were estimated for patients with AML versus healthy volunteers. A 51.2% decrease in k_a and 5.1% increase in F1 were estimated when quizartinib was administered under fed conditions versus fasted conditions. A strong CYP3A inhibitor use produced a 13.6% increase in F1 and a 44.1% decrease in CL. Quizartinib V_c, V_{p1}, and Q_1 were predicted to increase with increasing body surface area and age, with V_c predicted to decrease with increasing albumin.

All fixed- and random-effect parameters for quizartinib were estimated with good precision (<29.1% RSE [relative standard error expressed as a percent]), except the estimated fractional change for fed status on F1 in study AC220-019 (52.0% RSE). The magnitude of the IIV was high for D1 (69.3% CV [coefficient of variation expressed as a percent]), absorption lag time (62.0% CV), and CL (55.1% CV). The estimated magnitude of the IIV for the remainder of PK parameters was relatively modest, ranging from 24.8% CV (IIV in Q_1) to 39.7% CV (IIV in V_{p1}). The magnitude of RV ranged from 7.5% to 49.4% CV in healthy volunteers and from 19.4% to 52.6% CV in patients with AML for concentrations ranging from 1000 to 2.0 ng/mL.

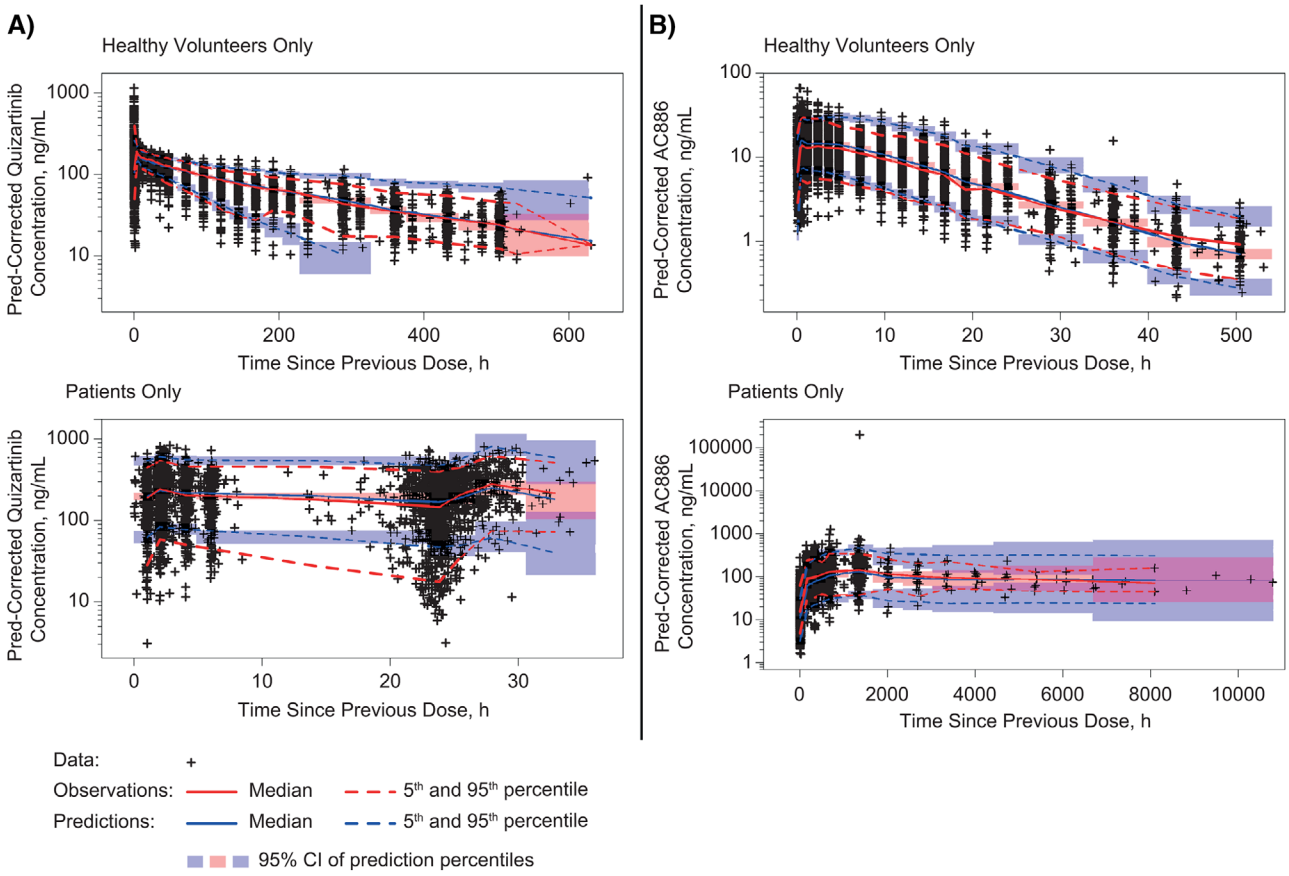

Figure 3. Prediction-corrected visual predictive checks plots for (A) quizartinib and (B) AC886.

Parameter estimates of the final model are shown in Table 3.

The final AC886 population PK model equations to describe parameter-covariate relationships are shown below in equations 8 and 9.

$$V_{cm_i} = 4.95 \times (1 + 1.92 \times flag_{STRCYP_i}) \quad (8)$$

$$CL_{m_i} = 4.09 \times (\frac{BSA_i}{1.9})^{1.60} \times [1 + (0.586 \times flag_{RACB_i}) + (0.106 \times flag_{STRCYP_i})] \quad (9)$$

where V_{cm_i} is the apparent central volume of distribution (L) of AC886 in the *i*th participant; $flag_{STRCYP_i}$ is the indicator variable for strong CYP3A inhibitor use (0 for no strong CYP3A inhibitor use, 1 for strong CYP3A inhibitor use); CL_{m_i} is the apparent clearance of AC886 (L/h); BSA_i is the body surface area (m^2); and $flag_{RACB_i}$ is the indicator variable for black/African American race (0 for non-black/African American participant; 1 for black/African American participant).

The CL_m is predicted to increase with increasing body surface area and to increase by 58.6% in black/African American patients with AML compared with patients of all other races. The CL_m and V_{cm} are predicted to increase by 10.6% and 192%, respectively, with concomitant strong CYP3A inhibitor use. Separate IIV terms for CL_m between healthy volunteers and patients with AML predicted a larger magnitude of IIV (64.1% CV) in patients with AML than in healthy volunteers (45.9% CV).

All fixed- and random-effect parameters were estimated with good precision (<27.7%). The magnitude of estimated IIV for V_{cm} was high (117% CV). The estimated RV for the refined final model was 26.3% CV and 41.2% CV for the healthy volunteer and AML patient populations, respectively. Parameter estimates of the final model are shown in Table 4.

pcVPC plots for quizartinib and AC886 are shown in Figure 3. The median and 5th and 95th percentile lines generally agree with the observed data across the observed concentration range. Goodness-of-fit plots for the final population models exhibited good concordance between the observed and model-predicted quizartinib concentrations in healthy volunteers (Figure S1) and in patients with AML (Figure S2), as well as for AC886 concentrations in healthy volunteers (Figure S3) and in patients with AML (Figure S4). Individual plots of population- and individual-predicted

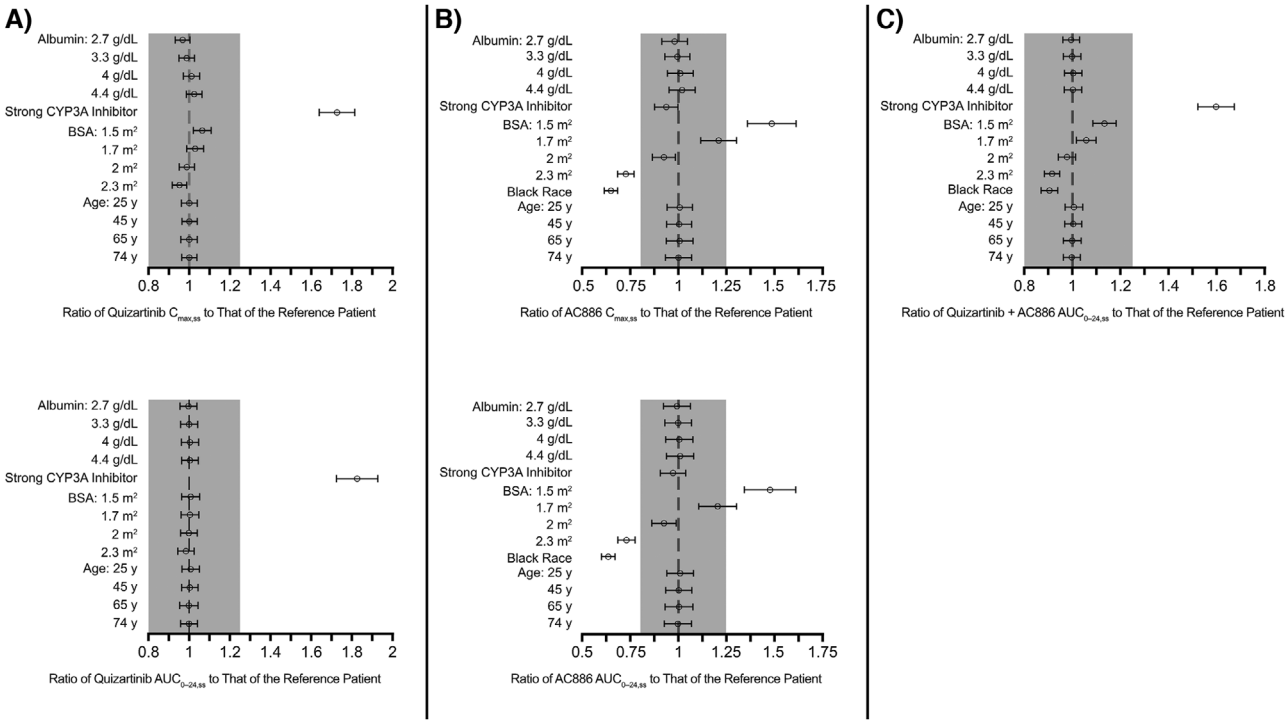

Figure 4. Impact of significant covariates on AUC and C_{max} of quizartinib, AC886, and sum of quizartinib and AC886. (A) Simulated quizartinib $C_{max,ss}$ and $AUC_{0\text{-}24,ss}$ ratios. (B) Simulated AC886 $C_{max,ss}$, and $AUC_{0\text{-}24,ss}$ ratios. (C) Simulated $AUC_{0\text{-}24,ss}$ ratios of the sum of quizartinib and AC886 for each individual compared with that of the reference patient with AML (60-mg once-daily dose). The reference patient with AML was defined as a patient with AML not receiving a strong CYP3A inhibitor, with albumin of 3.7 g/dL and BSA of 1.9 m^2. Open circle represents the median value, and horizontal line represents 90%CI based on 1000 simulations. BSA, body surface area; CYP, cytochrome P450.

concentrations versus time showed generally good agreement (data on file; Daiichi Sankyo, Inc.).

Forest plots derived from simulations using covariates included in the final population PK model were generated to demonstrate covariate effects on PK exposures in patients with AML. A total of 1000 simulations were conducted for each covariate effect using virtual patients with specified covariate attributes, taking into account the uncertainty in the fixed-effect model parameters (using results from a bootstrap with 1000 replicates). Ratios of simulated quizartinib $C_{max,ss}$ and $AUC_{0\text{-}24,ss}$ in these virtual patients, compared with the reference patient with AML, are shown in Figure 4A. Effects of covariates on quizartinib exposure were all <20%, except for the concomitant use of CYP3A inhibitors, which resulted in 82% and 72% increases in quizartinib AUC and C_{max}, respectively.

Black/African American participants had approximately 35% lower AC886 exposure than participants of other races, and BSA at extremely low (5th percentile) and high (95th percentile) values resulted in >20% change in AC886 exposures (Figure 4B). However, these effects on the total exposure (sum of quizartinib and AC886; Figure 4C) were not clinically meaningful because their magnitudes were <20%.

Of all statistically significant covariates identified and included in the PK models, concomitant strong CYP3A inhibitor use exhibited the largest effect on the exposure of quizartinib, whereas the individual effects of every other covariate were <20%. Thus, these results suggest that concomitant strong CYP3A inhibitor use is the only factor that may require dose reductions in the clinical setting to maintain quizartinib concentrations within the therapeutic window and mitigate the risk of QTcF increase.

Discussion

Population PK models for quizartinib and its active metabolite, AC886, were developed using pooled data from 649 healthy volunteers and patients with AML enrolled across 6 phase 1, 1 phase 2, and 1 phase 3 studies. This analysis population represented a comprehensive framework that encompassed both densely sampled and sparsely sampled PK data collected following single- and multiple-dose oral administration of 20 to 90 mg/day of quizartinib doses.

A 3-compartment PK model for quizartinib was optimal, particularly in describing the full PK profiles collected in healthy volunteers enrolled in the single-dose studies, in which intensive blood sampling was

performed up to 504 hours postdose. The PK of AC886 was sufficiently characterized with a 2-compartment model. An absorption model employing zero-order and first-order input for quizartinib into the central compartment with lag time was found to most appropriately capture the absorption phase of quizartinib. In turn, when the estimated PK of quizartinib was used to sequentially model AC886 PK, the fraction of quizartinib metabolized to AC886 was fixed to 50% to avoid parameter identifiability issues, which is a common approach implemented to model parent and metabolite concentrations when only the parent drug is dosed.[14] For both quizartinib and AC886, separate residual error terms were used for healthy volunteers and patients, with AML to account for the higher variability observed in studies of patients with AML.

In analyzing parent and metabolite PK data, simultaneous and sequential approaches have both been used as valid methods.[15-18] PK data included in this analysis were derived only from studies in which quizartinib was orally administered. Therefore, estimation of both F_{MET} (parent-to-metabolite conversion fraction) and metabolite central compartment parameters (CL_m and V_m) is not feasible. This is known as the unidentifiability problem in either simultaneous or sequential modeling.[14] To resolve this issue, we fixed F_{MET} at 0.5 on the basis of the noncompartmental analysis result of study 2689-CL-2004, in which the geometric mean ratio of AC886 $AUC_{0\text{-}24,ss}$ to quizartinib $AUC_{0\text{-}24,ss}$ was 0.544 for the 30-mg cohort and 0.485 for the 60-mg cohort.

Among the statistically significant covariates identified, only strong CYP3A inhibitor use produced a clinically meaningful effect on quizartinib exposure. Model-estimated effects for strong CYP3A inhibitor use included a 13.6% higher F1 and a 44.1% decrease in CL for quizartinib, as well as a 10.6% higher CL_m and an approximately 2-fold increase in V_{cm} for AC886. The net effect of CYP3A inhibitor use on the exposures of quizartinib and AC886 described by the model corroborate the changes in exposures observed in a dedicated drug-drug interaction study.[8] The BSA and black/African American race effects showed >20% change in AC886 exposures. However, these were not considered clinically meaningful because the changes in the sum of quizartinib and AC886 concentration were within the 0.8 to 1.25 range, assuming 1:1 potency. Considering that the actual potency ratio could be higher for some of the clinical responses,[12] the effects of these covariate on AC886 exposures were not considered clinically relevant.

The following covariates were tested but found not to have a significant influence: sex, race, estimated glomerular filtration rate (eGFR), baseline liver function variables (including AST, ALT, ALP, and TBIL), and concomitant use of acid-reducing agents (including proton pump inhibitors, H_2 blockers, and antacids). Lack of any detectable effect of gastric acid-reducing agents confirmed the results of the phase 1 study, which showed that lansoprazole did not result in a meaningful change in the bioavailability of quizartinib.[19] There was also no effect of mild or moderate hepatic impairment on quizartinib or AC886 PK based on baseline liver function values. No significant effect of eGFR on quizartinib CL was observed. This finding is consistent with the results of the human absorption, distribution, metabolism, and excretion study, which showed that renal excretion was a minor route of elimination for quizartinib, with mean excretion from urine < 2% (data on file; Daiichi Sankyo, Inc.). In the population PK analysis data set, individual eGFR values were calculated using the Modification of Diet in Renal Disease study equation[20] and ranged up to 379 mL/min/1.73 m^2. Because such a high eGFR value might not be physiologically relevant, a sensitivity analysis was conducted by rerunning the final quizartinib population PK model with the original eGFR values (ie, individual values up to 379 mL/min/1.73 m^2) or eGFR values capped at 120 mL/min/1.73 m^2.[21] The NONMEM objective function value decreases from these runs were 0.326 ($P = .568$) and 2.37 ($P = .124$), respectively, thereby confirming no effect of eGFR on quizartinib clearance.

Quizartinib exposure was lower in patients with AML than in healthy volunteers, described by a 40.1% reduction in F1 and an 8.2% increase in CL. However, the rate of absorption was approximately 2-fold higher in patients with AML than in healthy volunteers, which was evident in observed T_{max} values of approximately 2 and 4 hours, respectively. Although the exact reason for altered absorption in patients with relapsed/refractory AML is unknown, changes in the gastrointestinal tract may be secondary to the effects of prior chemotherapy. It is also worth noting that patient studies (2689-CL-0011, 2689-CL-2004, and QuANTUM-R) used relatively sparse PK sampling (0, 1, 2, 4, 6, and 24 hours postdose on PK sampling days of cycle 1 days 1 and 15) compared with the healthy volunteer studies, in which dense PK sampling was conducted (eg, 22 points over 480 hours in study AC220-014). Although the modeling analysis results were consistent with observed data, there remains a possibility that such a conclusion is data driven and may have resulted from differences in PK sampling schemes for patient studies versus healthy volunteer studies.

During the covariate model development, body size measures showed a statistically significant effect on quizartinib PK parameters. However, the level of significance was higher for body surface area than for body weight during the univariate analysis. Because body surface area and weight are highly correlated with each other, body surface area was selected for inclusion in

the PK model. After the final population PK model was established, a sensitivity analysis was conducted by replacing body surface area in the final model with body weight. The body weight model resulted in a 12-point-higher objective function value compared with that of the body surface area model. The effects of body surface area and body weight on exposures (AUC, C_{max}, C_{trough}) showed similar trends.

This analysis showed a significant effect of concomitant strong CYP3A inhibitors on quizartinib exposure. Of note, the effect of concomitant CYP3A inducers could not be adequately assessed in this analysis because of the lack of prevalent concomitant CYP3A4 inducer use in the study population. In the QuANTUM-R study, concomitant use of strong or moderate CYP3A4 inducers was prohibited because of a possible decrease in exposure of approximately 60% to 70% (data on file; Daiichi Sankyo, Inc.), but weak CYP3A4 inducers were allowed. Coadministration of strong CYP3A inhibitors or strong CYP3A4 inducers had similar effects on the PK of FLT3 inhibitors gilteritinib and midostaurin.[22-24] The observed increase in gilteritinib exposure with strong CYP3A inhibitor itraconazole was approximately 2.2-fold, and the strong CYP3A4 inducer rifampin decreased gilteritinib exposure by 30% versus gilteritinib alone.[24] Inhibition of CYP3A by ketoconazole increased midostaurin exposure by >10-fold, and induction of CYP3A4 by rifampicin decreased midostaurin exposure by >10-fold.[22,23] As such, the concomitant use of gilteritinib and a combined CYP3A4 and P-gp inducer should be avoided, and alternative therapies to strong CYP3A inhibitors should be considered.[25] Similarly, alternative therapies to strong CYP3A inhibitors should be considered with midostaurin, and the use of strong CYP3A4 inducers should be avoided.[26] To optimize quizartinib dosing, the starting quizartinib dose was reduced from 30 to 20 mg for those taking a concomitant strong CYP3A inhibitor in the QuANTUM-R study.

Conclusions

Population PK models were established and optimized for quizartinib and AC886 using data sets comprising healthy volunteers and patients with AML. Among the demographic and clinical covariates evaluated, concomitant use of strong CYP3A inhibitors was identified as the only significant covariate that is likely to produce a meaningful effect on the overall exposure of quizartinib, with an 82% increase in the median $AUC_{0\text{-}24,ss}$ and a 72% increase in median $C_{max,ss}$ of quizartinib. These results support the clinical recommendation for a quizartinib dose reduction with the concomitant use of strong CYP3A inhibitors in the clinical setting.

Conflicts of Interest

D. Kang is an employee and shareholder of Daiichi Sankyo, Inc. E. Ludwig, D. Jaworowicz, H. Huang, and J. Fiedler-Kelly are employees of Cognigen Corporation, which provided consulting services and received financial support from Daiichi Sankyo, Inc., to perform the analyses described. J. Cortes received grants and personal fees from Daiichi Sankyo, Inc., Astellas, Novartis, Pfizer, Jazz Pharmaceuticals, and Biopath Holdings and grants from Amphivena. Mercus. S. Ganguly received research support from Daiichi Sankyo, Inc., and personal fees from Seattle Genetics. S. Khaled received travel support from Daiichi Sankyo, Inc. A. Krämer received travel support from the University of Heidelberg. M. Levis received grants and personal fees from Astellas and FujiFilm and grants from Agios and Amgen. G. Martinelli received personal fees from Amgen, Daiichi Sankyo, Inc., Celgene, AbbVie, Novartis, and Jazz Pharmaceuticals. A. Perl received grants, personal fees, and travel support from Daiichi Sankyo, Inc., and Astellas, grants and personal fees from Novartis, and grants from FujiFilm, and nonfinancial support from Arog. N. Russell has nothing to disclose. M. Abutarif is an employee and shareholder of Daiichi Sankyo, Inc. Y. Choi and O. Yin are employees of Daiichi Sankyo, Inc. J. Mendell was employed by Daiichi Sankyo, Inc., at the time the work was conducted. Medical editorial assistance was provided by Scott Battle, PhD (Medical Expressions, a Nucleus Global company), funded by Daiichi Sankyo in accordance with Good Publication Practice guidelines.

Funding

This study was funded by Daiichi Sankyo, Inc.

Data-Sharing Statement

Deidentified individual participant data and applicable supporting clinical trial documents may be available on request at https://www.clinicalstudydatarequest.com. In cases in which clinical trial data and supporting documents are provided pursuant to our company policies and procedures, Daiichi Sankyo, Inc., will continue to protect the privacy of our clinical trial participants. Details on data-sharing criteria and the procedure for requesting access can be found at this web address: https://www.clinicalstudydatarequest.com/Study-Sponsors/Study-Sponsors-DS.aspx.

References

1. Daver N, Schlenk RF, Russell NH, Levis MJ. Targeting FLT3 mutations in AML: review of current knowledge and evidence. *Leukemia*. 2019;33(2):299.
2. Levis M. FLT3 mutations in acute myeloid leukemia: what is the best approach in 2013? *Hematology Am Soc Hematol Educ Program*. 2013;2013:220-226.
3. Boissel N, Cayuela JM, Preudhomme C, et al. Prognostic significance of FLT3 internal tandem repeat in patients with de novo acute myeloid leukemia treated with reinforced courses of chemotherapy. *Leukemia*. 2002;16(9):1699-1704.

4. Ravandi F, Kantarjian H, Faderl S, et al. Outcome of patients with FLT3-mutated acute myeloid leukemia in first relapse. *Leuk Res*. 2010;34(6):752-756.
5. Cortes J, Perl AE, Dohner H, et al. Quizartinib, an FLT3 inhibitor, as monotherapy in patients with relapsed or refractory acute myeloid leukaemia: an open-label, multicentre, single-arm, phase 2 trial. *Lancet Oncol*. 2018;19(7):889.
6. Cortes JE, Tallman MS, Schiller GJ, et al. Phase 2b study of 2 dosing regimens of quizartinib monotherapy in FLT3-ITD mutated, relapsed or refractory AML. *Blood*. 2018;132(5):598-607.
7. Cortes JE, Khaled S, Martinelli G, et al. Quizartinib versus salvage chemotherapy in relapsed or refractory FLT3-ITD acute myeloid leukaemia (QuANTUM-R): a multicentre, randomised, controlled, open-label, phase 3 trial. *Lancet Oncol*. 2019;20(7):984-997.
8. Li J, Kankam M, Trone D, Gammon G. Effects of CYP3A inhibitors on the pharmacokinetics of quizartinib, a potent and selective FLT3 inhibitor, and its active metabolite. *Br J Clin Pharmacol*. 2019;85(9):2108-2117.
9. Sanga M, James J, Marini J, Gammon G, Hale C, Li J. An open-label, single-dose, phase 1 study of the absorption, metabolism and excretion of quizartinib, a highly selective and potent FLT3 tyrosine kinase inhibitor, in healthy male subjects, for the treatment of acute myeloid leukemia. *Xenobiotica*. 2017;47(10):856-869.
10. Aikawa T, Togashi N, Iwanaga K, et al. Quizartinib, a selective FLT3 inhibitor, maintains antileukemic activity in preclinical models of RAS-mediated midostaurin-resistant acute myeloid leukemia cells. *Oncotarget*. 2020;11(11):943-955.
11. Zarrinkar PP, Gunawardane RN, Cramer MD, et al. AC220 is a uniquely potent and selective inhibitor of FLT3 for the treatment of acute myeloid leukemia (AML). *Blood*. 2009;114(14):2984-2982.
12. Kang D, Lin K, Ludwig E, Yin O. Concentration-QT analysis of quizartinib in patients with relapsed/refractory AML. *J Pharmacokinet Pharmacodyn*. 2018;45(1):Abstract M-044.
13. Levis MJ, Cortes JE, Gammon GM, Trone D, Kang D, Li J. Laboratory and clinical investigations to identify the optimal dosing strategy for quizartinib (AC220) monotherapy in FLT3-Itd-positive (+) relapsed/refractory (R/R) acute myeloid leukemia (AML). *Blood*. 2016;128(22):4042-4042.
14. Bertrand J, Laffont CM, Mentre F, Chenel M, Comets E. Development of a complex parent-metabolite joint population pharmacokinetic model. *AAPS J*. 2011;13(3):390-404.
15. Dickinson L, Boffito M, Back D, et al. Sequential population pharmacokinetic modeling of lopinavir and ritonavir in healthy volunteers and assessment of different dosing strategies. *Antimicrob Agents Chemother*. 2011;55(6):2775-2782.
16. Lehr T, Staab A, Tillmann C, et al. Population pharmacokinetic modelling of NS2330 (tesofensine) and its major metabolite in patients with Alzheimer's disease. *Br J Clin Pharmacol*. 2007;64(1):36-48.
17. Li H, Sun Y, Yu J, Liu C, Liu J, Wang Y. Semimechanistically based modeling of pembrolizumab time-varying clearance using 4 longitudinal covariates in patients with non-small cell lung cancer. *J Pharm Sci*. 2019;108(1):692-700.
18. Zhang L, Beal SL, Sheiner LB. Simultaneous vs. sequential analysis for population PK/PD data I: best-case performance. *J Pharmacokinet Pharmacodyn*. 2003;30(6):387-404.
19. Li J, Trone D, Mendell J, O'Donnell P, Cook N. A drug-drug interaction study to assess the potential effect of acid-reducing agent, lansoprazole, on quizartinib pharmacokinetics. *Cancer Chemother Pharmacol*. 2019;84(4):799-807.
20. Stevens LA, Coresh J, Greene T, Levey AS. Assessing kidney function–measured and estimated glomerular filtration rate. *N Engl J Med*. 2006;354(23):2473-2483.
21. Niu J, Scheuerell C, Mehrotra S, et al. Parent-metabolite pharmacokinetic modeling and pharmacodynamics of veliparib (ABT-888), a PARP Inhibitor, in patients with BRCA 1/2 -mutated cancer or PARP-sensitive tumor types. *J Clin Pharmacol*. 2017;57(8):977-987.
22. Dutreix C, Lorenzo S, Wang Y. Comparison of two endogenous biomarkers of CYP3A4 activity in a drug-drug interaction study between midostaurin and rifampicin. *Eur J Clin Pharmacol*. 2014;70(8):915-920.
23. Dutreix C, Munarini F, Lorenzo S, Roesel J, Wang Y. Investigation into CYP3A4-mediated drug-drug interactions on midostaurin in healthy volunteers. *Cancer Chemother Pharmacol*. 2013;72(6):1223-1234.
24. Levis M, Smith C, Litzow M, et al. Drug-drug interaction potential of gilteritinib in healthy subjects and patients with relapsed/refractory acute myeloid leukemia. Paper presented at: 2017 Annual Meeting of the European Hematology Society 2018; Madrid, Spain.
25. Xospata® (gilteritinib) [package insert]. Northbrook, IL: Astellas Pharma US Inc.; 2018.
26. Rydapt® (midostaurin) [package insert]. East Hanover, NJ: Novartis Pharmaceuticals Corporation; 2017.
27. Li J, Holmes M, Kankam M, Trone D, Mendell J, Gammon G. Effect of food on the pharmacokinetics of quizartinib. *Clin Pharmacol Drug Dev*. 2020;9(2):277-286.
28. Sandmaier BM, Khaled S, Oran B, Gammon G, Trone D, Frankfurt O. Results of a phase 1 study of quizartinib as maintenance therapy in subjects with acute myeloid leukemia in remission following allogeneic hematopoietic stem cell transplant. *Am J Hematol*. 2018;93(2):222-231.

Supplemental Information

Additional supplemental information can be found by clicking the Supplements link in the PDF toolbar or the Supplemental Information section at the end of web-based version of this article.